INTERNATIONAL JOURNAL FOR NUMERICAL METHODS IN ENGINEERING
Int. J. Numer. Meth. Engng 2007; **69**:2036–2057
Published online 15 August 2006 in Wiley InterScience (www.interscience.wiley.com). DOI: 10.1002/nme.1825

An uncoupled directional damage model for fibred biological soft tissues. Formulation and computational aspects

B. Calvo, E. Peña, M. A. Martinez and M. Doblaré*, †

Group of Structural Mechanics and Materials Modeling, Aragón Institute of Engineering Research, University of Zaragoza, María de Luna, 3. E-50018 Zaragoza, Spain

SUMMARY

In this paper we present a fully three-dimensional finite-strain damage model for fibrous soft tissue. Continuum damage mechanics is used to describe the softening behaviour of soft tissues under large deformation. The structural model is formulated using the concept of internal variables that provides a very general description of materials involving irreversible effects. We considered the internal variables associated to damage to correspond to separated contributions of the matrix and fibres. In order to show clearly the performance of the constitutive model, we present 3D simulations of the behaviour of the human medial collateral ligament and of a coronary artery. Results show that the model is able to capture the typical stress–strain behaviour observed in fibrous soft tissues and seems to confirm the soundness of the proposed formulation. Copyright 2006 John Wiley & Sons, Ltd.

Received 2 March 2006; Revised 1 June 2006; Accepted 2 June 2006

KEY WORDS: continuum damage; anisotropic hyperelastic material; fibred materials; soft tissues

1. INTRODUCTION

Biological soft tissues are subjected to large deformations with negligible volume changes and show an anisotropic mechanical response due to their internal structure. The extra-cellular matrix is composed of a network of collagen fibrils and elastin fibres embedded in a viscous and isotropic ground substance. Their mechanical stiffness and ultimate tensile strength have been shown to depend on the length of collagen fibrils; longer fibrils permit a greater number of inter-fibrillar connections, resulting in a more efficient force transmission. Experimental evidence shows that tissues subjected to axial tensile stresses [1, 2] have a typical non-linear response, with an initial

*Correspondence to: M. Doblaré, Mechanical Engineering Department, University of Zaragoza, Agustín de Betancourt Building, María de Luna, s/n. E-50018 Zaragoza, Spain.
†E-mail: mdoblare@unizar.es

Contract/grant sponsor: CICYT; contract/grant numbers: DPI2003-09110-C02-01, DPI2004-07410-C03-01, FIS2005-05020-C03-03

low stiffness toe region, a linear part with approximately constant stiffness, and a third region corresponding to progressive failure of the composing fibres.

Usually, the description of the constitutive behaviour of this type of material relies on the identification of an appropriate strain energy density function from which stress–strain relations and local elasticity tensors are derived [3]. Even though different strain energy density functions have proved to be successful for particular applications and for describing many of the material properties, their use is limited, in most cases, to the range of physiological loads. In fact, most finite element applications have been limited to analysing the mechanical response of soft tissue into the toe and linear regions (References [4–6] for ligaments, Reference [7] for arteries and Reference [8] for cornea), that is, the behaviour of soft tissue under normal physiological loads.

Only a few of them describe the mechanical behaviour of soft tissue in the failure region. Hurschler *et al*. [9] and Liao and Belkoff [10] have proposed respective formulations to describe damage in soft tissue; however, these models have been restricted to damage of only the collagenous component. Natali *et al*. [11] presented a transversely isotropic elasto-damage constitutive model for tendons. It results, however, in non-symmetric algorithmic tangent moduli with an elevated computational cost. Hokanson and Yazdani [12] presented a constitutive model for arteries that included damage, but they did not present any example nor application. Similarly, Arnoux *et al*. [13] and Schechtman and Bader [14] presented theoretical phenomenological damage models for ligaments and tendons. Rodriguez *et al*. [15] introduced a stochastic-structurally based damage model for fibrous soft tissues.

Non-physiological loads drive soft tissue to damage that arises from two possible mechanisms. One would be tear or plastic deformation of fibres. Tear of fibres is consistent with Hurschler's micromechanical model for ligament behaviour that includes fibre failure [9]. Another possible mechanism for the observed ligament laxity could be biochemical degradation of the extracellular matrix from protease release associated with the observed cellular necrosis [16]. A structural damage model that considers separated contributions on damage from the matrix and fibres would be therefore desirable. Up to the authors' knowledge, only Rodríguez *et al*. [15] take into account different damage processes for matrix and fibres. However, damage of the fibrous part is incorporated through the statistical distribution of the deformation at the fully extended length of collagen fibre bundles. This implies that model calibration requires working at two scale levels, so the numerical fit is laborious and the computational cost in finite element simulations expensive.

In this paper, we present a fully three-dimensional finite strain anisotropic damage model for fibred soft tissues. The structural model is formulated within the framework of non-linear continuum damage mechanics [17] using the concept of internal variables that provides a very general description of materials involving irreversible effects [18–20]. This framework was initially used to model the mechanical behaviour of isotropic elastomers [20–22]. We have considered a material reinforced by two families of fibres continuously distributed in a compliant solid isotropic matrix [23]. The internal variables associated to damage correspond to separated contributions of the matrix and fibres. Since the mechanical response of biological tissues is almost isochoric [24], we assume uncoupled volumetric and deviatoric responses over any range of deformation [25]. This is achieved by a local multiplicative decomposition of the deformation gradient into volume-preserving and dilatational parts. The description of the constitutive model is established in the reference configuration (Lagrangian approach) and we also express the tangent operator for FE implementations that results symmetric.

Several numerical examples under finite strains are presented in order to illustrate the good performance and the physical mechanisms inherent to the constitutive model. This model has been

DOI: 10.1002/nme

applied to simulate the damage process on this kind of tissues in some clinical applications. This is the case of the behaviours of the human medial collateral ligament (MCL) and coronary arteries. Results show that the model is able to capture the typical stress–strain behaviour observed in fibrous soft tissues and seems to confirm the soundness of the proposed formulation.

The paper is organized as follows. In Section 2 the constitutive equations of anisotropic hyperelastic materials are briefly revised. In Section 3 the proposed anisotropic damage model for biological soft tissue is presented. Applications of the described approach to some examples are included in Section 4. First, a simple geometry example is used to validate and easily compare different methodologies. Next, the simulation of the behaviour of the human MCL of the knee in non-physiological conditions is discussed. Two examples for coronary arteries, balloon angioplasty an arterial clamping are also presented. Finally, Section 5 includes some concluding remarks.

2. LAGRANGIAN DESCRIPTION OF HYPERELASTIC FIBRED MATERIALS

Many biological tissues such as ligaments or blood vessels are subjected to large deformations with negligible volume changes, that is, only quasi-isochoric ($J \approx 1$) motions are possible. These materials are composed of a matrix material (ground substance) and one or more families of fibres. When reinforced by only one family of fibres, they have a single preferred direction and are usually modelled as *transversely isotropic hyperelastic materials* [4] while in the case of two families of fibres they are modelled as *fully anisotropic hyperelastic materials* [26]. This section provides a brief review of basic concepts in finite deformation continuum mechanics and constitutive behaviour of fibred materials.

Consider a continuum body with reference configuration Ω_0 at the initial reference time $t = 0$. Then, an assumed motion $\boldsymbol{\chi}$ maps this configuration to the current configuration Ω at each time t. Hence, a point $\mathbf{X} \in \Omega_0$ transforms to a point $\mathbf{x} \in \Omega$, where $\mathbf{X}$ and $\mathbf{x}$ define the respective positions of a particle in the reference and current configurations relative to a fixed set of axes. The direction of a fibre at a point $\mathbf{X} \in \Omega_0$ is defined by a unit vector field $\mathbf{m}_0(\mathbf{X})$, $|\mathbf{m}_0| = 1$. It is usually assumed that, under deformation, the fibre moves with the material points of the continuum body. Therefore, the stretch λ of the fibre defined as the ratio between its lengths at the deformed and reference configurations can be expressed as

$$\lambda \mathbf{m}(\mathbf{x}, t) = \mathbf{F}(\mathbf{X}, t)\mathbf{m}_0(\mathbf{X}) \tag{1}$$

where $\mathbf{m}$ is the unit vector of the fibre in the deformed configuration

$$\lambda^2 = \mathbf{m}_0 \cdot \mathbf{F}^{\mathrm{T}}\mathbf{F} \cdot \mathbf{m}_0 = \mathbf{m}_0 \cdot \mathbf{C}\mathbf{m}_0 \tag{2}$$

In (1), (2) $\mathbf{F} = \mathrm{d}\mathbf{x}/\mathrm{d}\mathbf{X}$ and $\mathbf{C} = \mathbf{F}^{\mathrm{T}}\mathbf{F}$ are the standard deformation gradient and the corresponding right Cauchy–Green strain measure. A multiplicative decomposition of $\mathbf{F}$ into *volume-changing* (*dilational*) and *volume-preserving* (*distortional*) parts is usually established as in References [25, 27]

$$\mathbf{F} = J^{1/3}\bar{\mathbf{F}}, \quad \mathbf{C} = J^{2/3}\bar{\mathbf{C}} \tag{3}$$

The introduced kinematics for one family of fibres can be applied to other fibre families in an analogous manner. We shall denote a second preferred fibre direction by the unit vector field $\mathbf{n}_0(\mathbf{X})$.

To characterize isothermal processes, we postulate the existence of a unique decoupled representation of the strain-energy density function Ψ [28]. Because of the directional dependence on

DOI: 10.1002/nme

the deformation, we require that the function Ψ explicitly depends on both the right Cauchy–Green tensor $\mathbf{C}$ and the fibres direction, $\mathbf{m}_0$ and $\mathbf{n}_0$, in the reference configuration. Since the sign of $\mathbf{m}_0$ and $\mathbf{n}_0$ is not relevant, Ψ must be an even function of $\mathbf{m}_0$ and $\mathbf{n}_0$ and so it may be expressed by $\Psi = \Psi(\mathbf{C}, \mathbf{M}, \mathbf{N})$ where $\mathbf{M} = \mathbf{m}_0 \otimes \mathbf{m}_0$ and $\mathbf{N} = \mathbf{n}_0 \otimes \mathbf{n}_0$ are structural tensors [23]. Based on the kinematic description (3), the free energy can be written in decoupled form as

$$\Psi(\mathbf{C}) = \Psi_{\text{vol}}(J) + \bar{\Psi}(\bar{\mathbf{C}}, \mathbf{M}, \mathbf{N}) \tag{4}$$

where $\Psi_{\text{vol}}(J)$ and $\bar{\Psi}(\bar{\mathbf{C}}, \mathbf{M}, \mathbf{N})$ are given scalar-valued functions of J, $\bar{\mathbf{C}}$, $\mathbf{m}_0$ and $\mathbf{n}_0$, respectively, that describe the volumetric and isochoric responses of the material [26]. In terms of the strain invariants [23] Ψ can be written as

$$\begin{aligned}\Psi = \Psi_{\text{vol}}(J) + \bar{\Psi}(&\bar{I}_1(\bar{\mathbf{C}}), \bar{I}_2(\bar{\mathbf{C}}), \bar{I}_4(\bar{\mathbf{C}}, \mathbf{m}_0), \bar{I}_5(\bar{\mathbf{C}}, \mathbf{m}_0),\\ &\bar{I}_6(\bar{\mathbf{C}}, \mathbf{n}_0), \bar{I}_7(\bar{\mathbf{C}}, \mathbf{n}_0), \bar{I}_8(\bar{\mathbf{C}}, \mathbf{m}_0, \mathbf{n}_0), \bar{I}_9(\mathbf{m}_0, \mathbf{n}_0))\end{aligned} \tag{5}$$

with $\bar{I}_1$ and $\bar{I}_2$ the first two modified strain invariants of the symmetric modified Cauchy–Green tensor $\bar{\mathbf{C}}$ (note that $I_3 = J$ and $\bar{I}_3 = 1$). Finally, the pseudo-invariants $\bar{I}_4, \ldots, \bar{I}_9$ characterize the constitutive response of the fibres [23]:

$$\begin{aligned}&\bar{I}_4 = \mathbf{C} : \mathbf{M}, \quad \bar{I}_5 = \mathbf{C}^2 : \mathbf{M}\\ &\bar{I}_6 = \mathbf{C} : \mathbf{N}, \quad \bar{I}_7 = \mathbf{C}^2 : \mathbf{N}\\ &\bar{I}_8 = (\mathbf{m}_0 \cdot \mathbf{n}_0)\mathbf{m}_0 \cdot \bar{\mathbf{C}}\mathbf{n}_0, \quad \bar{I}_9 = (\mathbf{m}_0 \cdot \mathbf{n}_0)^2\end{aligned} \tag{6}$$

While the invariant $\bar{I}_4$ and $\bar{I}_6$ have a clear physical meaning, the square of the stretch λ in the fibre direction, the influence of $\bar{I}_5$, $\bar{I}_7$ and $\bar{I}_8$ is difficult to evaluate due to the high correlation among the invariants. For this reason and the lack of sufficient experimental data it is usual to not include these invariants in the definition of Ψ [23]. Finally, $\bar{I}_9$ does not depend of the deformation and therefore is not relevant to the constitutive behaviour.

We now define the constitutive equation for compressible hyperelastic materials in the standard form

$$\mathbf{S} = 2\,\frac{\partial \Psi(\mathbf{C}, \mathbf{M}, \mathbf{N})}{\partial \mathbf{C}} = \mathbf{S}_{\text{vol}} + \bar{\mathbf{S}} \tag{7}$$

where the second Piola–Kirchhoff stress $\mathbf{S}$ consists of a purely volumetric contribution and a purely isochoric one. The associated decoupled elasticity tensor may be written as

$$\mathbb{C} = \mathbb{C}_{\text{vol}} + \mathbb{C}_{\text{iso}} = 2\,\frac{\partial \mathbf{S}_{\text{vol}}}{\partial \mathbf{C}} + 2\,\frac{\partial \bar{\mathbf{S}}}{\partial \mathbf{C}} \tag{8}$$

The Cauchy stress tensor $\boldsymbol{\sigma}$ and the elasticity tensor in the spatial description $_{\mathbb{C}}$ is $1/J$ times the push-forward of $\mathbf{S}$ or $_{\mathbb{C}}$, respectively [26, 29]

$$\boldsymbol{\sigma} = J^{-1}\boldsymbol{\chi}_*(\mathbf{S}), \quad _{\mathbb{C}} = J^{-1}\boldsymbol{\chi}_*(\mathbb{C}) \tag{9}$$

For a more detailed derivation of the material and spatial elasticity tensors for completely incompressible or compressible fibred hyperelastic materials and their explicit expressions, see i.e. Reference [23] or [26].

DOI: 10.1002/nme

3. ANISOTROPIC DAMAGE MODEL

The aim of this section is to formulate a three-dimensional and rate-independent anisotropic damage model in the large strain domain able to describe the reduction in the mechanical stiffness of soft tissues when strains over the physiological range cause the progressive failure of the fibrils network. The structural model is formulated within the framework of non-linear continuum damage mechanics and uses the concept of internal variables which provides a very general description of materials involving irreversible effects. It is a purely phenomenological approach, which describes the macroscopic constitutive behaviour for stresses exceeding the elastic limit of the tissue [18, 19]. The model assumes separated contributions of the matrix and fibres.

3.1. Anisotropic damage at finite strains

Damage is assumed to affect only the isochoric elastic part of the deformation, as proposed by Simo [20]. The free energy density can then be written in a decoupled form, such as

$$\Psi(\mathbf{C}, \mathbf{M}, \mathbf{N}, D_{\mathrm{m}}, D_{\mathrm{f}}) = \Psi_{\mathrm{vol}}(J) + (1 - D_{\mathrm{m}})\bar{\Psi}_0^{\mathrm{m}}(\bar{\mathbf{C}}) + (1 - D_{\mathrm{f}})\bar{\Psi}_0^{\mathrm{f}}(\bar{\mathbf{C}}, \mathbf{M}, \mathbf{N}) \tag{10}$$

where $\mathbf{M}$ and $\mathbf{N}$ are the structural tensors, $\Psi_{\mathrm{vol}}(J)$ is a strictly convex function (with the minimum at $J = 1$) which describes the volumetric elastic response, $\bar{\Psi}_0^{\mathrm{m}}$ denotes the isochoric effective strain energy density of the undamaged material, which describes the elastic response of the matrix, and $\bar{\Psi}_0^{\mathrm{f}}$ denotes the isochoric effective strain energy of the undamaged material, which describes the isochoric elastic response of the fibres. The factors $(1 - D_{\mathrm{m}})$ and $(1 - D_{\mathrm{f}})$ are known as reduction factors [20], where the internal variables $D_{\mathrm{m}} \in [0, 1]$ and $D_{\mathrm{f}} \in [0, 1]$ are normalized scalars referred to as damage variables for the matrix and fibres, respectively.

In order to obtain the stress we first differentiate (10) with respect to time. Using the chain rule we find

$$\dot{\Psi} = \frac{\mathrm{d}\Psi_{\mathrm{vol}}(J)}{\mathrm{d}J}\,\dot{J} + (1 - D_{\mathrm{m}})\,\frac{\partial \bar{\Psi}_0^{\mathrm{m}}}{\partial \bar{\mathbf{C}}} : \dot{\bar{\mathbf{C}}} - \bar{\Psi}_0^{\mathrm{m}}\dot{D}_{\mathrm{m}} + (1 - D_{\mathrm{f}})\frac{\partial \bar{\Psi}_0^{\mathrm{f}}}{\partial \bar{\mathbf{C}}} : \dot{\bar{\mathbf{C}}} - \bar{\Psi}_0^{\mathrm{f}}\dot{D}_{\mathrm{f}} \tag{11}$$

As a particularization of the Clausius–Planck inequality we obtain the non-negative internal dissipation $\mathscr{D}_{\mathrm{int}}$ as [29]

$$\mathscr{D}_{\mathrm{int}} = \left(\mathbf{S} - J\,\frac{\mathrm{d}\Psi_{\mathrm{vol}}(J)}{\mathrm{d}J}\,\mathbf{C}^{-1} - J^{-2/3}\mathbb{P} : (1 - D_{\mathrm{m}})2\,\frac{\partial \bar{\Psi}_0^{\mathrm{m}}}{\partial \bar{\mathbf{C}}} - J^{-2/3}\mathbb{P} : (1 - D_{\mathrm{f}})2\frac{\partial \bar{\Psi}_0^{\mathrm{f}}}{\partial \bar{\mathbf{C}}}\right) : \frac{\dot{\mathbf{C}}}{2} + \bar{\Psi}_0^{\mathrm{m}}\dot{D}_{\mathrm{m}} + \bar{\Psi}_0^{\mathrm{f}}\dot{D}_{\mathrm{f}} \geqslant 0 \tag{12}$$

and using standard arguments in continuum constitutive mechanics the second Piola–Kirchhoff stress $\mathbf{S}$ may be written as the sum of a purely volumetric contribution and a purely isochoric one

$$\mathbf{S} = \mathbf{S}_{\mathrm{vol}} + (1 - D_{\mathrm{m}})\bar{\mathbf{S}}_0^{\mathrm{m}} + (1 - D_{\mathrm{f}})\bar{\mathbf{S}}_0^{\mathrm{f}} \tag{13}$$

DOI: 10.1002/nme

with

$$\bar{\mathbf{S}}_0^{\mathrm{m}} = J^{-2/3}\,\mathrm{DEV}\left[2\,\frac{\partial \bar{\Psi}_0^{\mathrm{m}}(\bar{\mathbf{C}})}{\partial \bar{\mathbf{C}}}\right], \quad \bar{\mathbf{S}}_0^{\mathrm{f}} = J^{-2/3}\,\mathrm{DEV}\left[2\,\frac{\partial \bar{\Psi}_0^{\mathrm{f}}(\bar{\mathbf{C}}, \mathbf{M}, \mathbf{N})}{\partial \bar{\mathbf{C}}}\right] \tag{14}$$

and from the same arguments

$$\mathscr{D}_{\mathrm{int}}^{\mathrm{m}} = f_{\mathrm{m}}\dot{D}_{\mathrm{m}} \geqslant 0, \quad \mathscr{D}_{\mathrm{int}}^{\mathrm{f}} = f_{\mathrm{f}}\dot{D}_{\mathrm{f}} \geqslant 0 \tag{15}$$

with

$$f_{\mathrm{m}} = \bar{\Psi}_0^{\mathrm{m}}(\bar{\mathbf{C}}) \geqslant 0, \quad f_{\mathrm{f}} = \bar{\Psi}_0^{\mathrm{f}}(\bar{\mathbf{C}}, \mathbf{M}, \mathbf{N}) \geqslant 0 \tag{16}$$

The dissipation inequalities (15) clearly show that damage is a dissipative process. The quantities f_{m}, f_{f} denote the thermodynamic driving forces which govern the damage evolution of matrix and fibres, respectively, and have the meaning of the effective strain energy $\bar{\Psi}_0^{\mathrm{m}}$, $\bar{\Psi}_0^{\mathrm{f}}$ of matrix and fibres, respectively. f_{m}, f_{f} are conjugate of the internal variables D_{m}, D_{f} according to

$$f_{\mathrm{m}} = \bar{\Psi}_0^{\mathrm{m}}(\bar{\mathbf{C}}) = -\frac{\partial \Psi}{\partial D_{\mathrm{m}}} \quad \text{and} \quad f_{\mathrm{f}} = \bar{\Psi}_0^{\mathrm{f}}(\bar{\mathbf{C}}, \mathbf{M}, \mathbf{N}) = -\frac{\partial \Psi}{\partial D_{\mathrm{f}}} \tag{17}$$

Note that when we consider uncoupled behaviour between the two families of fibres, we can define different damage evolutions for each family ($D_{\mathrm{f_m}}$ and $D_{\mathrm{f_n}}$) replacing in (10) the term $(1 - D_{\mathrm{f}})\bar{\Psi}_0^{\mathrm{f}}$ by $\sum_{i=1,2}\{(1 - D_{\mathrm{f}_i})\bar{\Psi}_0^{\mathrm{f}_i}\}$.

3.2. Damage evolution

The evolution of the damage parameters D_{m} and D_{f} is characterized by an irreversible equation of evolution as follows. We define Ξ_s^{m}, Ξ_s^{f} by the expression [20]

$$\Xi_s^{\mathrm{m}} = \sqrt{2\bar{\Psi}_0^{\mathrm{m}}(\bar{\mathbf{C}}(s))} \quad \text{and} \quad \Xi_s^{\mathrm{f}} = \sqrt{2\bar{\Psi}_0^{\mathrm{f}}(\bar{\mathbf{C}}(s))} \tag{18}$$

where $\bar{\mathbf{C}}(s)$ is the modified right Cauchy–Green tensor at time s. Now, let Ξ_t^{m}, Ξ_t^{f} be the maximum values of Ξ_s^{m}, Ξ_s^{f} over the past history up to current time t, that is [20]

$$\Xi_t^{\mathrm{m}} = \max_{s\in(-\infty,t)} \sqrt{2\bar{\Psi}_0^{\mathrm{m}}(\bar{\mathbf{C}}(s))} \quad \text{and} \quad \Xi_t^{\mathrm{f}} = \max_{s\in(-\infty,t)} \sqrt{2\bar{\Psi}_0^{\mathrm{f}}(\bar{\mathbf{C}}(s))} \tag{19}$$

We define a damage criterion for the ground substance or matrix in the strain space by the condition that, at any time t of the loading process, the following expression is fulfilled [20]:

$$\phi_{\mathrm{m}}(\mathbf{C}(t), \Xi_t^{\mathrm{m}}) = \sqrt{2\bar{\Psi}_0^{\mathrm{m}}(\bar{\mathbf{C}}(t))} - \Xi_t^{\mathrm{m}} \leqslant 0 \tag{20}$$

The equation $\phi_{\mathrm{m}}(\mathbf{C}(t), \Xi_t^{\mathrm{m}}) = 0$ defines a damage surface in the strain space. Denoting by $N_{\mathrm{m}} := \partial\phi_{\mathrm{m}}/\partial\mathbf{C}$, the normal to the damage surface in that space, the following alternative situations may occur:

$$\phi_{\mathrm{m}} < 0 \quad \text{or} \quad \phi_{\mathrm{m}} = 0 \quad \text{and} \quad \begin{cases} \mathbf{N}_{\mathrm{m}} : \dot{\mathbf{C}} < 0 \\ \mathbf{N}_{\mathrm{m}} : \dot{\mathbf{C}} = 0 \\ \mathbf{N}_{\mathrm{m}} : \dot{\mathbf{C}} > 0 \end{cases} \tag{21}$$

DOI: 10.1002/nme

Borrowing a terminology typically found in plasticity [30, 31], we speak of unloading, neutral loading, or loading from a damage state, respectively. Finally, the evolution of the damage variable D_{m} is specified by the irreversible rate equation

$$\frac{\mathrm{d}D_{\mathrm{m}}}{\mathrm{d}t} = \begin{cases} \bar{h}_{\mathrm{m}}(\Xi^{\mathrm{m}}, D_{\mathrm{m}})\dot{\Xi}^{\mathrm{m}} & \text{if } \phi = 0 \quad \text{and} \quad \mathbf{N}_{\mathrm{m}} : \dot{\mathbf{C}} > 0 \\ 0 & \text{otherwise} \end{cases} \tag{22}$$

Here $\bar{h}_{\mathrm{m}}(\Xi^{\mathrm{m}}, D_{\mathrm{m}})$ is a given function that characterizes the damage evolution in the material.

If $\bar{h}_{\mathrm{m}}(\Xi^{\mathrm{m}}, D_{\mathrm{m}})$ is independent of D_{m}, the deviatoric part of the second Piola–Kirchoff stress tensor for the matrix may be expressed in the following form:

$$\bar{\mathbf{S}}^{\mathrm{m}}(t) = \bar{g}_{\mathrm{m}}(\Xi^{\mathrm{m}}_t) 2 \frac{\partial \bar{\Psi}^{\mathrm{m}}_0(\bar{\mathbf{C}}(t))}{\partial \mathbf{C}} \tag{23}$$

with $\bar{h}_{\mathrm{m}}(\Xi^{\mathrm{m}}) = -\mathrm{d}\bar{g}_{\mathrm{m}}(\Xi^{\mathrm{m}})/\mathrm{d}\Xi$.

The damage process of collagen fibrils D_{f} is due to their progressive rupture along the direction of the fibrils. In this case, the damage evolution is identical to that of the matrix, changing the damage function in (22) to $\bar{h}_{\mathrm{f}}(\Xi^{\mathrm{f}}, D_{\mathrm{f}})$ and $\bar{\Psi}^{\mathrm{f}}_0$ and Ξ^{f} in the damage criterion (20). In addition, the deviatoric part of the second Piola–Kirchoff stress tensor for the fibres may be expressed in the following form:

$$\bar{\mathbf{S}}^{\mathrm{f}}(t) = \bar{g}_{\mathrm{f}}(\Xi^{\mathrm{f}}_t) 2 \frac{\partial \bar{\Psi}^{\mathrm{f}}_0(\bar{\mathbf{C}}(t))}{\partial \mathbf{C}} \tag{24}$$

with $\bar{h}_{\mathrm{f}}(\Xi^{\mathrm{m}}) = -\mathrm{d}\bar{g}_{\mathrm{f}}(\Xi^{\mathrm{f}})/\mathrm{d}\Xi$.

To completely determine the damage model, it still remains to specify the functions $\bar{g}_{\mathrm{m}}(\Xi^{\mathrm{m}})$ and $\bar{g}_{\mathrm{f}}(\Xi^{\mathrm{f}})$, or equivalently, $\bar{h}_{\mathrm{m}}$ and $\bar{h}_{\mathrm{f}}$. Such a determination should be made on the basis of available experimental data.

3.3. Decoupled representation of the elasticity tensor

We note that the evolution of the stress tensor is completely determined by (13), so making use of the chain rule we have [26]

$$\dot{\bar{\mathbf{S}}}^{\mathrm{m}} = \begin{cases} [\bar{g}_{\mathrm{m}}\bar{\mathbb{C}}^{\mathrm{m}}_0 - \bar{g}'_{\mathrm{m}}\bar{\mathbf{S}}^{\mathrm{m}}_0 \otimes \bar{\mathbf{S}}^{\mathrm{m}}_0] : \dfrac{\dot{\mathbf{C}}}{2} & \text{if } \phi = 0 \quad \text{and} \quad \mathbf{N}_{\mathrm{m}} : \dot{\mathbf{C}} > 0 \\ \bar{g}_{\mathrm{m}}\bar{\mathbb{C}}^{\mathrm{m}}_0 : \dfrac{\dot{\mathbf{C}}}{2} & \text{otherwise} \end{cases} \tag{25}$$

$$\dot{\bar{\mathbf{S}}}^{\mathrm{f}} = \begin{cases} [\bar{g}_{\mathrm{f}}\bar{\mathbb{C}}^{\mathrm{f}}_0 - \bar{g}'_{\mathrm{f}}\bar{\mathbf{S}}^{\mathrm{f}}_0 \otimes \bar{\mathbf{S}}^{\mathrm{f}}_0] : \dfrac{\dot{\mathbf{C}}}{2} & \text{if } \phi = 0 \quad \text{and} \quad \mathbf{N}_{\mathrm{f}} : \dot{\mathbf{C}} > 0 \\ \bar{g}_{\mathrm{f}}\bar{\mathbb{C}}^{\mathrm{f}}_0 : \dfrac{\dot{\mathbf{C}}}{2} & \text{otherwise} \end{cases} \tag{26}$$

with $\bar{g}'_{\mathrm{m}} = \mathrm{d}\bar{g}_{\mathrm{m}}/\mathrm{d}\Xi^{\mathrm{m}} = -\bar{h}_{\mathrm{m}}$ and $\bar{g}'_{\mathrm{f}} = \mathrm{d}\bar{g}_{\mathrm{f}}/\mathrm{d}\Xi^{\mathrm{f}} = -\bar{h}_{\mathrm{f}}$.

The volumetric contribution to the elasticity tensor is defined by (8) and the isochoric contribution includes damage and is, by analogy with (8), divided into matrix and fibres contributions

DOI: 10.1002/nme

defined as

$$\bar{\mathbb{C}}^{\mathrm{m}}(t) = \begin{cases} \bar{g}_{\mathrm{m}}\bar{\mathbb{C}}_0^{\mathrm{m}} - \bar{g}'_{\mathrm{m}}\bar{\mathbf{S}}_0^{\mathrm{m}} \otimes \bar{\mathbf{S}}_0^{\mathrm{m}} & \text{if } \phi = 0 \quad \text{and} \quad \mathbf{N}_{\mathrm{m}} : \dot{\mathbf{C}} > 0 \\ \bar{g}_{\mathrm{m}}\bar{\mathbb{C}}_0^{\mathrm{m}} & \text{otherwise} \end{cases} \tag{27}$$

and

$$\bar{\mathbb{C}}^{\mathrm{f}}(t) = \begin{cases} \bar{g}_{\mathrm{f}}\bar{\mathbb{C}}_0^{\mathrm{f}} - \bar{g}'_{\mathrm{f}}\bar{\mathbf{S}}_0^{\mathrm{f}} \otimes \bar{\mathbf{S}}_0^{\mathrm{f}} & \text{if } \phi = 0 \quad \text{and} \quad \mathbf{N}_{\mathrm{f}} : \dot{\mathbf{C}} > 0 \\ \bar{g}_{\mathrm{f}}\bar{\mathbb{C}}_0^{\mathrm{f}} & \text{otherwise} \end{cases} \tag{28}$$

So, the elasticity tensor in the material description is obtained as

$$\mathbb{C} = \mathbb{C}_{\mathrm{vol}} + \bar{\mathbb{C}}^{\mathrm{m}} + \bar{\mathbb{C}}^{\mathrm{f}} \tag{29}$$

4. EXAMPLES

The anisotropic damage model proposed above has been implemented in ABAQUS 6.5-1 through UMAT Fortran subroutine.

In all the examples, the damage functions proposed for matrix and fibres, respectively, correspond to the expressions

$$\bar{g}_{\mathrm{m}}(\Xi_t^{\mathrm{m}}) = \begin{cases} 1 & \text{if } \Xi_t^{\mathrm{m}} < \psi_{\min}^{\mathrm{m}} \\ \dfrac{1 - \exp^{\beta^{\mathrm{m}}(\Xi_t^{\mathrm{m}} - \psi_{\max}^{\mathrm{m}})}}{1 - \exp^{\beta^{\mathrm{m}}(\psi_{\min}^{\mathrm{m}} - \psi_{\max}^{\mathrm{m}})}} & \text{if } \psi_{\min}^{\mathrm{m}} \leqslant \Xi_t^{\mathrm{m}} \leqslant \psi_{\max}^{\mathrm{m}} \\ 0 & \text{if } \Xi_t^{\mathrm{m}} > \psi_{\max}^{\mathrm{m}} \end{cases} \tag{30}$$

$$\bar{g}_{\mathrm{f}}(\Xi_t^{\mathrm{f}}) = \begin{cases} 1 & \text{if } \Xi_t^{\mathrm{f}} < \psi_{\min}^{\mathrm{f}} \\ \dfrac{1 - \exp^{\beta^{\mathrm{f}}(\Xi_t^{\mathrm{f}} - \psi_{\max}^{\mathrm{f}})}}{1 - \exp^{\beta^{\mathrm{f}}(\psi_{\min}^{\mathrm{f}} - \psi_{\max}^{\mathrm{f}})}} & \text{if } \psi_{\min}^{\mathrm{f}} \leqslant \Xi_t^{\mathrm{f}} \leqslant \psi_{\max}^{\mathrm{f}} \\ 0 & \text{if } \Xi_t^{\mathrm{f}} > \psi_{\max}^{\mathrm{f}} \end{cases} \tag{31}$$

where $\psi_{\min}^{\mathrm{m}}$ and $\psi_{\min}^{\mathrm{f}}$ are the strain energy at initial damage for matrix and fibres, respectively, $\psi_{\max}^{\mathrm{m}}$ and $\psi_{\max}^{\mathrm{f}}$ the strain energy at total damage for matrix and fibres, and β^{m} and β^{f} exponential parameters for matrix and fibres, respectively [11, 20].

4.1. Cyclic stretching of a thin perforated square plate

This example presents the numerical simulation of a thin perforated plate subjected to cyclic stretching along its longitudinal axis (uniaxial and biaxial tests). The geometry, boundary conditions and mesh are shown in Figure 1. Due to the symmetry only one quarter of the plate was considered in the finite element simulation. Two families of fibres defined in the X and Y direction were considered. The thin plate was subjected to two load steps. First, a triangular displacement history as shown Figure 2 (shaded line) was applied in direction X (uniaxial test). After that, other

DOI: 10.1002/nme

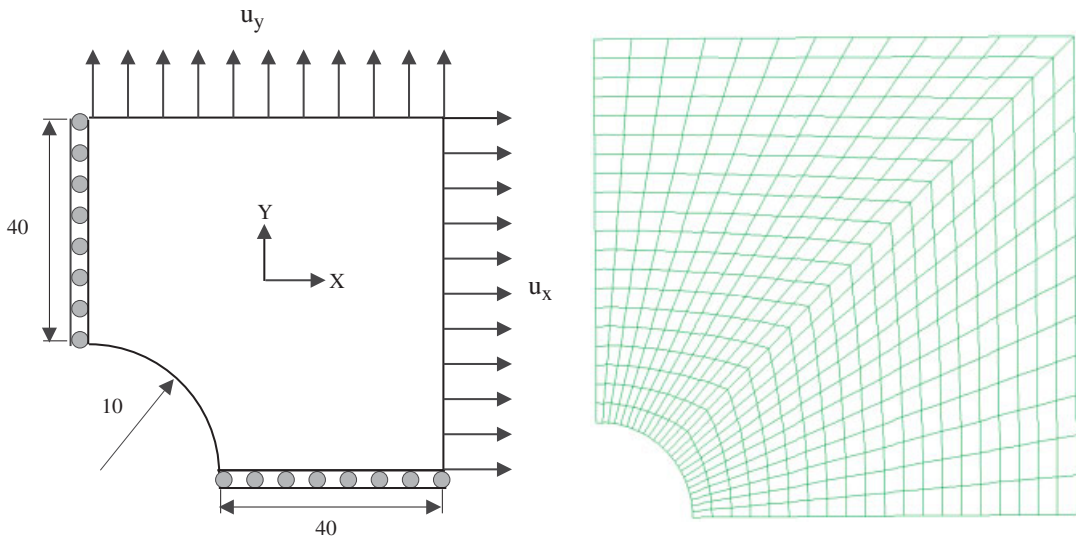

Figure 1. Thin perforated square plate. Geometry, boundary conditions and mesh.

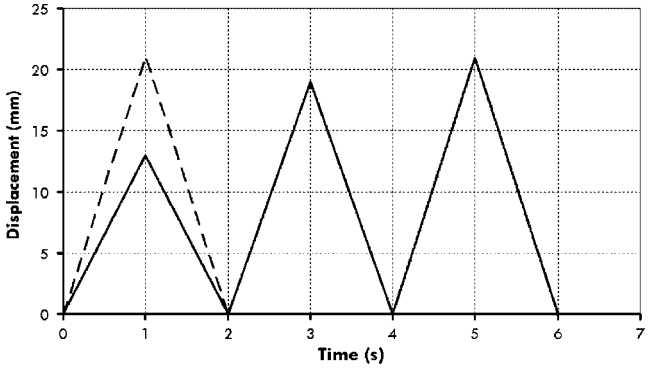

Figure 2. Load history in the thin plate problem.

triangular displacement history (pointed line in Figure 2) was applied in directions X and Y (biaxial test).

The particular form of the deviatoric functions $\bar{\Psi}_0^{\mathrm{m}}$ and $\bar{\Psi}_0^{\mathrm{f}}$ employed correspond to (32) and (33), respectively, and the volumetric part of the strain energy function was $\Psi_{\mathrm{vol}} = (1/D)\ln J^2$ [26]. The damage functions for the matrix and fibres were, respectively, (30) and (31). The material and damage parameters are shown in Table I.

$$\bar{\Psi}_0^{\mathrm{m}} = C_1(\bar{I}_1 - 3) + C_2(\bar{I}_2 - 3) \tag{32}$$

$$\bar{\Psi}_0^{\mathrm{f}} = \frac{C_3}{2C_4}(\exp^{C_4(\bar{I}_4-1)^2} - 1) \tag{33}$$

DOI: 10.1002/nme

Table I. Material and damage parameters for the thin plate (MPa).

C_1	C_2	C_3	C_4	D	
0.0274	0.0	6.4e-4	3.54	0.00039869	
$\psi^{\mathrm{m}}_{\mathrm{min}}$	$\psi^{\mathrm{m}}_{\mathrm{max}}$	β^{m}	$\psi^{\mathrm{f}}_{\mathrm{min}}$	$\psi^{\mathrm{f}}_{\mathrm{max}}$	β^{f}
0.1743	0.4974	2	0.103	0.998	0.4

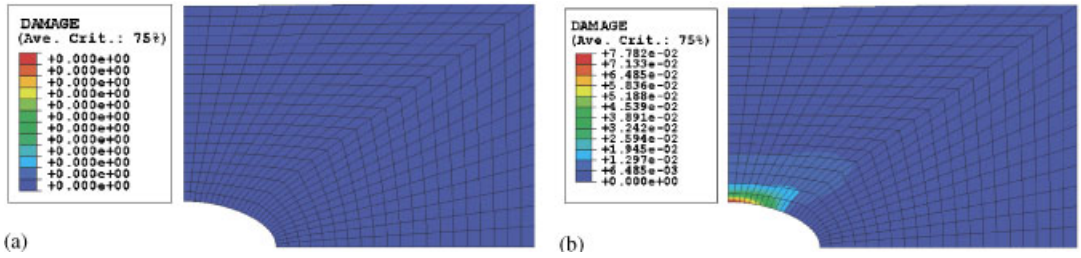

Figure 3. Damage contour plot in the deformed configuration at 14 mm of displacement: (a) matrix; and (b) fibres along X.

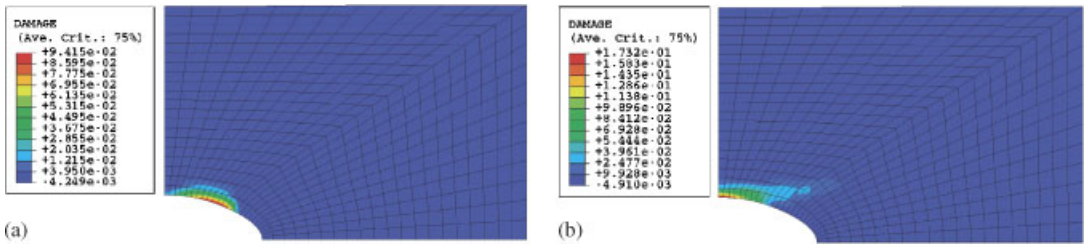

Figure 4. Damage contour plot in the deformed configuration at 19 mm of displacement: (a) matrix; and (b) fibres along X.

Figures 3–5 show the damage contours in the deformed configuration for the matrix and fibres during the first step for 14, 19 and 21 mm of displacement. In all the cases, it can be seen that, due to stress localization, the damage process is confined to a band near the perforation. Due to $\psi^{\mathrm{f}}_{\mathrm{min}}$ is obtained before $\psi^{\mathrm{m}}_{\mathrm{min}}$, peaks of damage are produced in the fibres in the two initial steps, see Figures 3 and 4. Obviously, the damage in the Y fibres is null. The peak values of damage for the matrix and X fibres resulted 0.0 and 0.0778 at 14 mm, 0.0941 and 0.1730 at 19 mm and 0.1398 and 0.2953 at 21 mm, Figure 5.

After the first step, a biaxial load was applied in X and Y directions. Due to the damage present in the matrix and X fibres, the material is anisotropic. So, the evolution of damage and stress is different in the two directions. In Figure 6, we can see the stress–strain evolution in X and Y directions for a point at the centre part of the plate with and without damage. It is shown that

DOI: 10.1002/nme

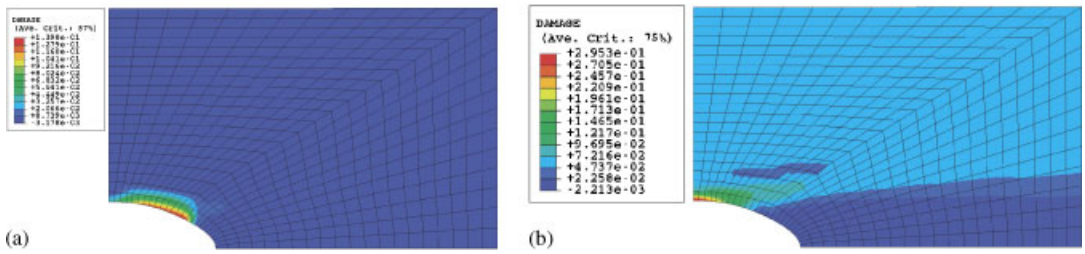

Figure 5. Damage contour plot in the deformed configuration at 21 mm of displacement: (a) matrix; and (b) fibres along X.

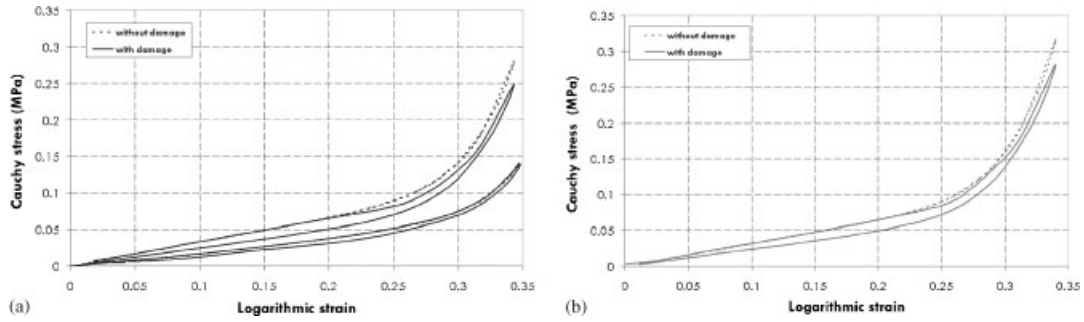

Figure 6. Stress–strain evolution in X and Y. Pointed line without damage and dashed line with damage: (a) σ_x; and (b) σ_y.

damage produces anisotropy in the material behaviour. In this case, there appear additional damage in the matrix and in both, X and Y fibres, see Figure 7.

4.2. Damage of human medial collateral ligament during valgus knee loading

Of all the knee ligaments, the MCL and the anterior cruciate ligaments (ACL) are the most frequent totally disrupted. Sports (sky, basketball, soccer) and traffic accidents are the most important causes of ligament injury. Clinical reports suggest that injuries in the MCL are located most commonly near the femoral insertion. Studies of ligament cutting and measurements of tissue load have shown that the MCL provides a primary restraint to valgus rotation and a secondary restraint to external rotation and anterior and posterior translations. Some results [32, 33] indicate that the largest strain in the MCL during valgus loading occurs near the femoral insertion in the fully extended knee, suggesting that this region may be most vulnerable to injury under these loading conditions. After injury, the healing process in ligaments results in the formation of fibrotic tissue. The structural, organizational, and mechanical properties of this healed tissue are inferior to normal MCL and depend of the amount of matrix and fibres injured [16, 34].

A sprain is defined as an acute injury of a ligament. Sprains are classified by severity on the basis of clinical examination or imaging. Grade I sprains are mild stretches with no discontinuity of the ligament and no clinically detectable increase in joint laxity. Grade II sprains are moderate

DOI: 10.1002/nme

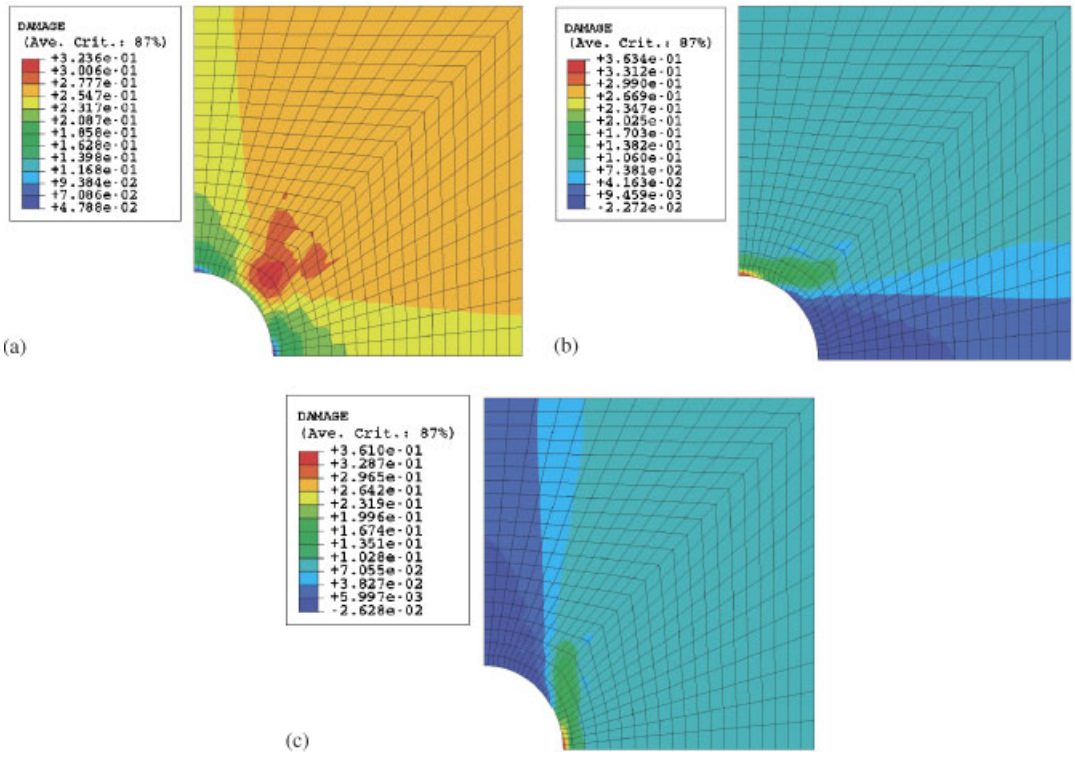

Figure 7. Damage contour plot in the deformed configuration after biaxial load: (a) matrix; (b) fibres along X; and (c) fibres along Y.

stretches in which some fibres are torn. Enough fibres remain intact so that the damaged ligament has not failed. These grade II sprains produce detectable abnormal laxity at the joint compared with the uninjured, contralateral side. Grade III sprains are severe and consist of a complete or nearly complete ligament disruption and result in significant joint laxity [34]. Obviously, we can only simulate Grade I and II injuries with the damage model presented herein since we use a continuum damage mechanics approach.

In this example, published experimental data from Weiss [35] until injury are compared to the results generated by the model presented herein. Even though experimental data are available only for monotonic load, we have studied a cyclic load. The material was loaded to a stretch of 1.0338 (3.3%), then unloaded, loaded again to a stretch of 1.037 (3.7%), unloaded and loaded again to a stretch of 1.055 [35], see Figure 9.

The particular form of the deviatoric function $\bar{\Psi}_0^{\mathrm{m}}$ and $\bar{\Psi}_0^{\mathrm{f}}$ employed corresponds to (32) and (33), respectively [36] and the volumetric part of the strain energy function was chosen as $\Psi_{\mathrm{vol}} = (1/D) \ln J^2$ [26].

In order to adjust the experimental data, we need first to estimate the parameters $\psi_{\min}$ and $\psi_{\max}$. It was assumed that $\psi_{\min}$ and $\psi_{\max}$ correspond to the strain energy associated to λ where the damage process begins and terminates, respectively, in the uniaxial test reported in Reference [35]. The maximum value of the strain energy corresponding to null damage in the matrix and fibres are

DOI: 10.1002/nme

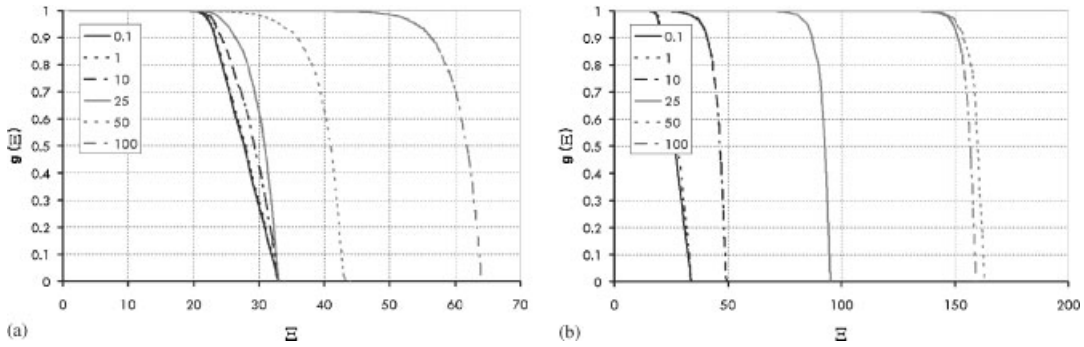

Figure 8. Damage master function for different values of β: (a) g_{m}; and (b) g_{f}.

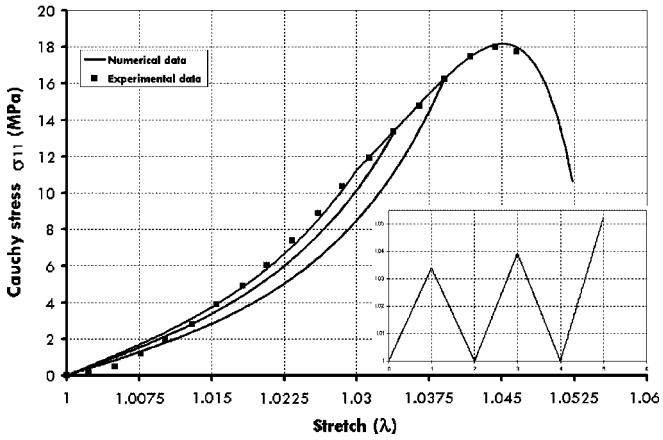

Figure 9. Numerical fit to the experimental data reported in Reference [35].

$\psi^{\mathrm{m}}_{\min} = 0.1635$ and $\psi^{\mathrm{f}}_{\min} = 0.4778$, and the minimum value of the strain energy corresponding to complete matrix and fibre damage are $\psi^{\mathrm{m}}_{\max} = 0.2974$ and $\psi^{\mathrm{f}}_{\max} = 1.3342$, respectively. Also, the parameters β_{m} and β_{f} affect the damage evolution. To estimate these beta parameters it is important to know the damage evolution laws for different values of β_{m} and β_{f} (Figure 8). The particular law in (30) and (31) for the damage variable allows to control the damage initiation as well as the rate at which damage develops with strain as shown in Figure 8. Lower values of β_{m} and β_{f} imply that most damage occurs at low stretches (energy) and the damage rate is constant when energy increases. β_{m} and β_{f} were adjusted to reproduce the damage region in the data reported by Weiss *et al.* [35].

The numerical fit to the experimental data reported in Reference [35] is shown in Figure 9. This figure exhibits the excellent fit obtained with the damage laws considered in (30) and (31). It shows the influence of Mullins effect on the global behaviour of the ligament. In order to obtain a complete model of damage in MCL we should fit experimental data in loading and unloading.

DOI: 10.1002/nme

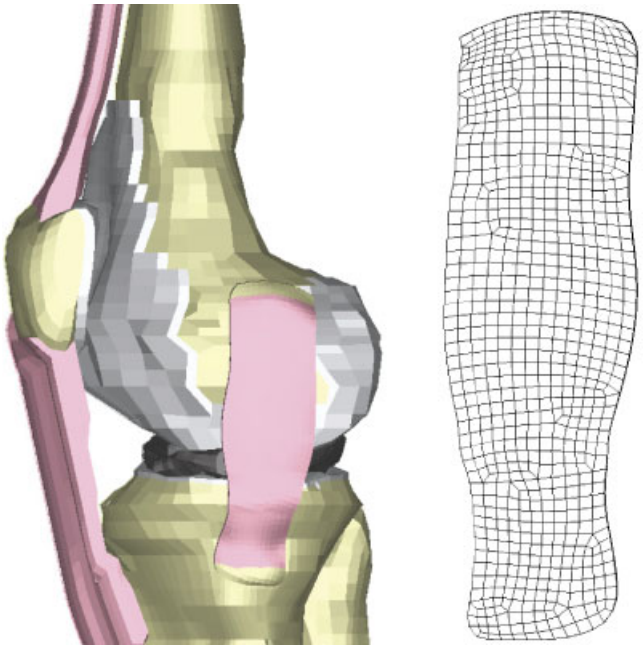

Figure 10. Finite element model of the human MCL.

Table II. Material and damage parameters for the MCL (MPa) fitted from Reference [35].

C_1	C_2	C_3	C_4	D	
5.05	0.0	46.0082	150.193	0.00039869	
$\psi^{\mathrm{m}}_{\mathrm{min}}$	$\psi^{\mathrm{m}}_{\mathrm{max}}$	β^{m}	$\psi^{\mathrm{f}}_{\mathrm{min}}$	$\psi^{\mathrm{f}}_{\mathrm{max}}$	β^{f}
0.1635	0.2974	20	0.4778	1.3342	0.01

To illustrate the performance of the damage model to capture the typical damage behaviour observed in ligaments, a model of the MCL was constructed to simulation its performance under a non-physiological valgus moment of 15Nm (the physiological value is about 10Nm), see Figure 10. The surface geometries of femur and tibia were reconstructed from a set of Computer Tomography scans, while for the MCL, magnetic resonance images (MRI) were used [6]. We used the previous data fit from the experimental results in Reference [35]. The material and damage parameters are shown in Table II and the damage functions are those defined in Equations (30) and (31).

Figure 11 shows the distribution of damage in the MCL for the valgus torque of 15 Nm. The peak values appeared in the femoral insertion and the contact region between ligament and tibial plate as indicated in previous experimental studies [37, 38]. Damage during valgus moment is usually produced in both regions and depends on age and the strain-rate. Additionally, we can see that the peak value in the fibres (0.675) is higher than for the matrix (0.15). This

DOI: 10.1002/nme

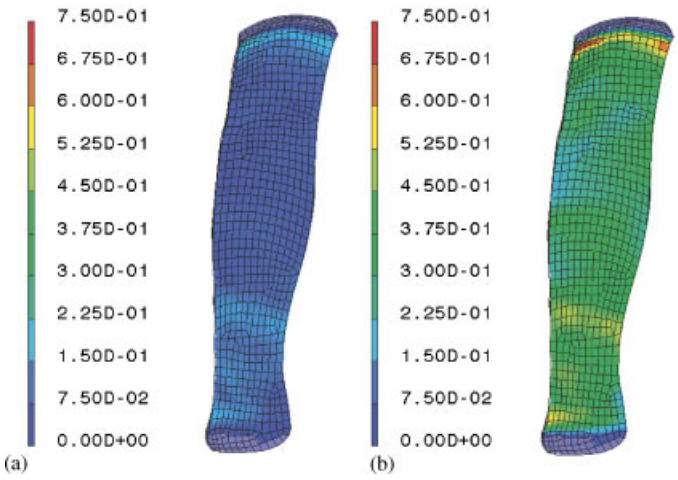

Figure 11. Distribution of the damage after valgus moment: (a) matrix; and (b) fibres.

is in agreement with the experimental results in sprains with Grade I and II without ligament tears [34].

4.3. Damage in arteries after balloon angioplasty

A considerable amount of effort has been devoted to the development of constitutive laws for the human artery in the normal physiological pressure range. These models aid to understand the behaviour of arteries under normal conditions and provide clues to the better understanding of disease genesis and progression [39]. A wide range of experimental work has been conducted to verify those mathematical models [2]. Only a few arterial models include the damage behaviour of arteries. Hokanson and Yazdami [12] presented an isotropic damage model for arteries while Gasser and Holzapfel [40] developed an elasto-plastic model for biological fibred tissues and used it to model balloon angioplasty [41].

There is also a great interest in the behaviour of arteries at higher pressures due to the widespread use of balloon angioplasty. Balloon angioplasty is performed at pressures much higher than the physiologic one and, as a result, structural changes due to tissue damage must be considered [41]. Finally, the existing finite deformation models of the artery with damage are also limited [12]. Oktay [42] presented the results of pressure–volume and extension experiments on bovine coronary arteries to determine damage from angioplasty in a cylindrical artery. The test artery was loaded in tension and with an internal pressure that did not induce damage. Next, the artery was inflated and deflated with a balloon to simulate angioplasty. Finally, the artery was reloaded with the same tension and internal pressure of step one to determine the amount of damage resulting from balloon inflation.

As the strain in the artery increases over the normal maximum physiological range, microtearing of collagen and elastin fibres is initiated [12]. The amount of damage is directly related to the magnitude of strain it experiences. Also, like natural rubber, the damage state is closely linked to the maximum strain the artery has previously experienced [12, 42]. That is, once an artery wall has been stretched to a certain strain it cannot be damaged further until it is stretched past

DOI: 10.1002/nme

Table III. Material (kPa) and damage parameters for the artery.

	C_1	C_2	C_3	C_4	D	γ
Media	2.7	0.0	0.0001	5.1	15.4	10°
Adventitia	27.4	0.0	0.0001	0.64	3.54	40°
$\psi^{\mathrm{m}}_{\min}$	$\psi^{\mathrm{m}}_{\max}$	β^{m}	$\psi^{\mathrm{f}}_{\min}$	$\psi^{\mathrm{f}}_{\max}$	β^{f}	
6.99	15.0	0.1	3.54	10	0.5	

this previous maximum strain. Under cyclic loading, it will follow the same stress–strain path until the maximum previous strain is exceeded [12]. This type of behaviour is called Mullins' effect [21, 43].

The main aim of this example is to reproduce the Oktay test for a cylindrical geometry corresponding to a human left anterior descending coronary artery (LAD) given in Reference [44] with internal and external radii $R_{\mathrm{i}} = 3.302$ and $R_{\mathrm{e}} = 3.795$ mm for the media layer and an external radii of $R_{\mathrm{e}} = 4.4042$ mm for the adventitia layer. The angle of the fibres with respect to the circumferential direction γ is shown in Table III (media). Due to the symmetry of the problem only half of the cylinder was considered in the finite element simulation. During the whole computation, the end faces of the artery were constrained to remain planar simulating a long vessel.

The volumetric part of the strain energy function was again $\Psi_{\mathrm{vol}} = (1/D) \ln J^2$ and the deviatoric functions corresponded to (34) [44]

$$\Psi_{\mathrm{iso}} = \frac{C_1}{2}(\overline{I}_1 - 3) + \frac{C_2}{2}(\overline{I}_2 - 3) + \frac{C_3}{2C_4}\{\exp[C_4(\overline{I}_4 - 1)^2] - 1\} \tag{34}$$

The elastic material parameters were borrowed from Reference [44] and the damage parameters were adopted from Reference [42]. Table III shows the material and damage parameters for the artery.

Figure 12 shows the maximal principal stress in the coronary artery after balloon angioplasty without and with consideration of damage. Since we did not consider the plaque, the maximum stresses appeared distributed in all the load region. The stress distribution was mainly circumferential, as expected from the radial balloon expansion. We can see in Figure 12 that wall elastic tissue limits (50–200 kPa) were exceeded, causing damage. It occurred in the entire media and intima as shown Figure 13. In the clinical context damage named as 'controlled vessel injury' [41] occurs predominantly in the media. We can see that the peak value is higher in the fibres (0.40) than in the matrix (0.123). This fact was experimentally observed by Chu and Blatz [45].

Results show that the model is able to capture the typical stress–strain behaviour observed in arteries and seems to confirm the soundness of the proposed formulation. However, and in order to obtain clinical conclusions, this example has several limitations. First, we simulated the arterial balloon angioplasty without the atheroma plaque. For this reason, damage in artery appeared distributed in a large region of the media. In addition, we used material and damage data available in

DOI: 10.1002/nme

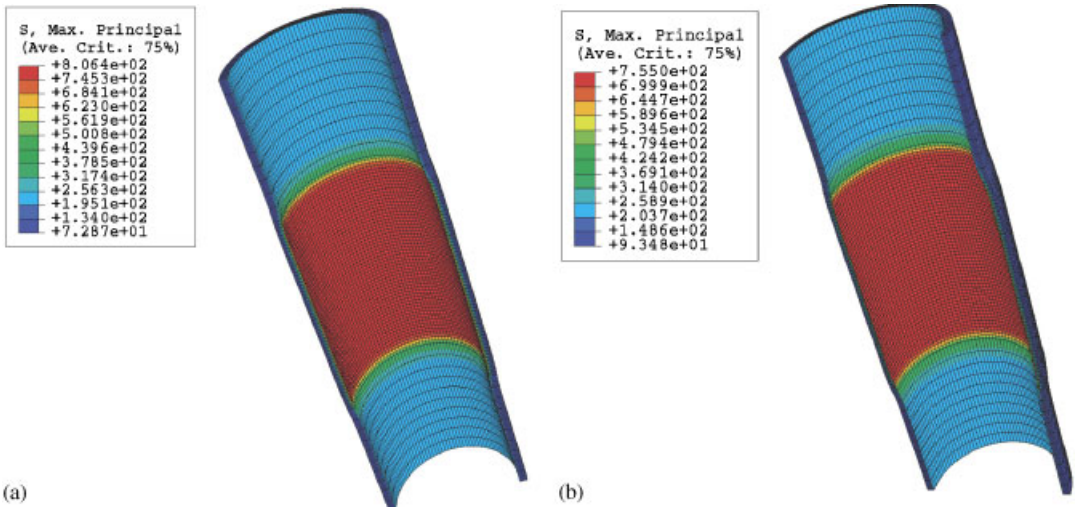

Figure 12. Maximal principal stresses after balloon angioplasty without and with damage (kPa): (a) without damage; and (b) with damage.

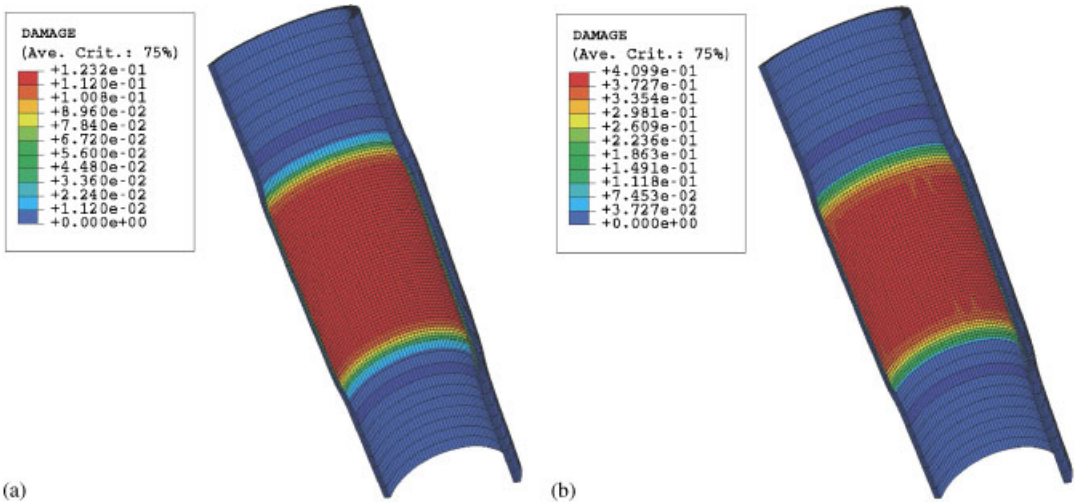

Figure 13. Distribution of damage after balloon angioplasty: (a) matrix damage; and (b) fibres damage.

the literature from different specimens. Despite these limitations, we have obtained results according to the damage phenomenon in arteries similar to those presented by other authors [12, 41, 42].

4.4. Damage after arterial clamping

Arterial clamps are designed to compress arteries during surgery so that blood flow is arrested. Arterial compression, however, may lead to injuries of the vessel wall, that have been associated

DOI: 10.1002/nme

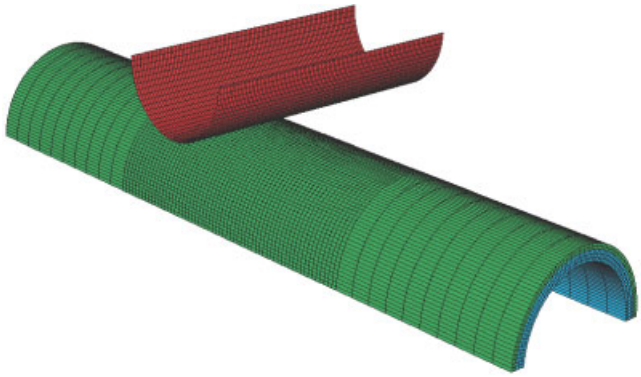

Figure 14. Geometry and mesh of the arterial clamping model.

to a variety of severe short-term complications [44]. The observed injuries range from mild damage, which involves only the intima, to severe damage with total disruption of the media, layer delaminations, and even total wall disruption and spontaneous occlusion of the vessel after the operation.

Appropriate numerical models may lead to substantial improvements of arterial clamp designs, and thus are of potential interest for surgeons and clamp suppliers. To the authors knowledge, only Gasser *et al*. [44] used a numerical method to study this clamping process. They developed a three-dimensional finite element model for arterial clamping using two-layered fibre-reinforced material, obtaining the stress distribution in the arterial wall during clamping. However, they used a non-linear elastic model that cannot capture the inelastic behaviour required to model the whole domain behaviour of the tissue. In that paper, they found that the media carried high axial stresses, so damage is mainly associated to the matrix.

In this section, we simulate the arterial clamping example presented by Gasser *et al*. [44]. The same geometry, material parameters, damage functions and boundary conditions of the previous section were used to model the arterial clamping. Following Gasser *et al*. [44], the arterial clamp was idealized as a rigid cylinder with a radius of 3.0 mm placed perpendicular to the axis of the artery (Figure 14). After arterial inflation to an internal physiological pressure of 13.33 kPa (100 mmHg), the frictionless interaction of the clamp with the artery was computed as a displacement-driven problem.

The results show that the circumferential stress in the wall tends to decrease while the axial stress in the media tends to increase (Figures 15 and 16). The circumferential stress decreased to 16 kPa (about 0.23 times lower than the physiological one) while the axial stress increased to 41.7 kPa in the media layer (about 3.6 times higher than the physiological stress). Similar trends were presented by Gasser *et al*. [44]. They obtained that the circumferential stress decreased up to 0.3 times with respect to the physiological stress being this value equal to four, for the axial stress increase. These differences is due to the stiffer behaviour in Gasser *et al*. where damage was not considered.

Since the media is not designed to carry high axial loads (this task corresponds to the adventitia) [44], the clamping process causes injury in the media. In this layer, the fibre distribution is mainly circumferential, so damage is associated to the matrix (Figure 17(a)) and not to the fibres (Figure 17(b)). This effect was observed in clinical results [46].

DOI: 10.1002/nme

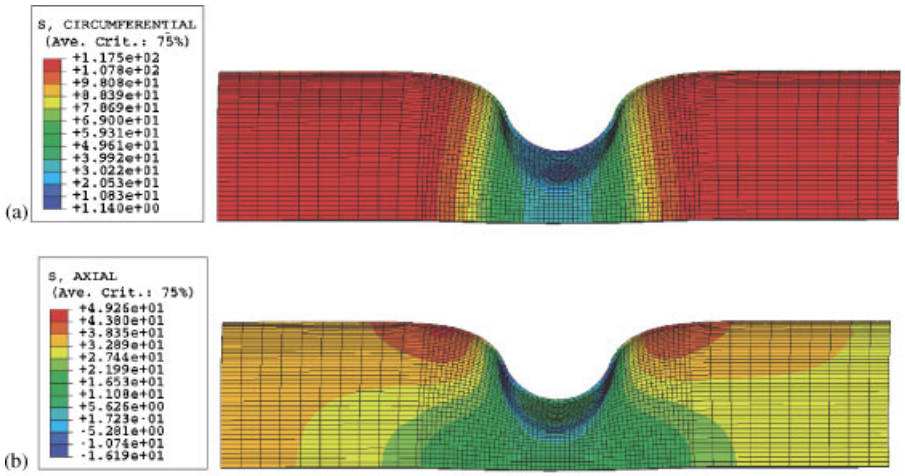

Figure 15. Distribution of the circumferential and axial stresses (kPa) in the adventitia at the final state of the clamping process including damage: (a) circumferential stress; and (b) axial stress.

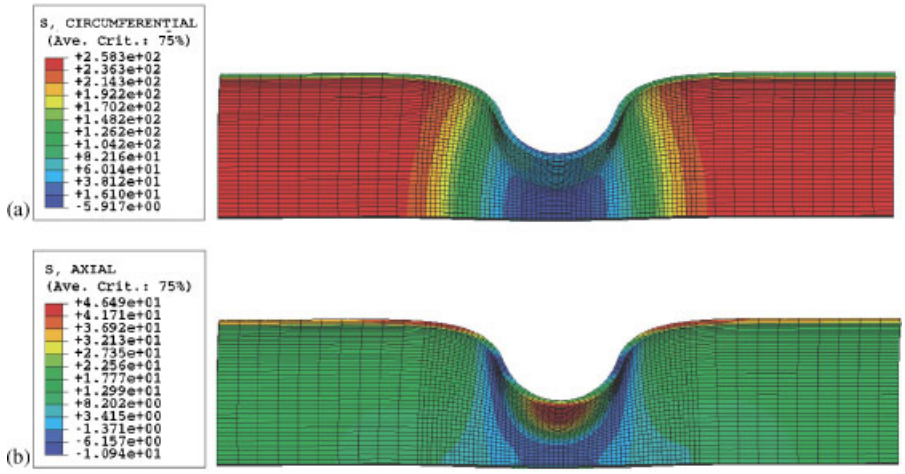

Figure 16. Distribution of the circumferential and axial stresses (kPa) in the media at the final state of the clamping process including damage: (a) circumferential stress; and (b) axial stress.

5. CONCLUSIONS

We have developed a fully 3D anisotropic constitutive damage model at finite strains for fibred materials as composites or soft biological tissues. Based on thermodynamic considerations, damage is characterized by the maximum value previously attained by the strain energy of the undamaged material. We use a local multiplicative decomposition of the deformation gradient into volume-preserving and dilatational parts that permits to model the incompressible properties

DOI: 10.1002/nme

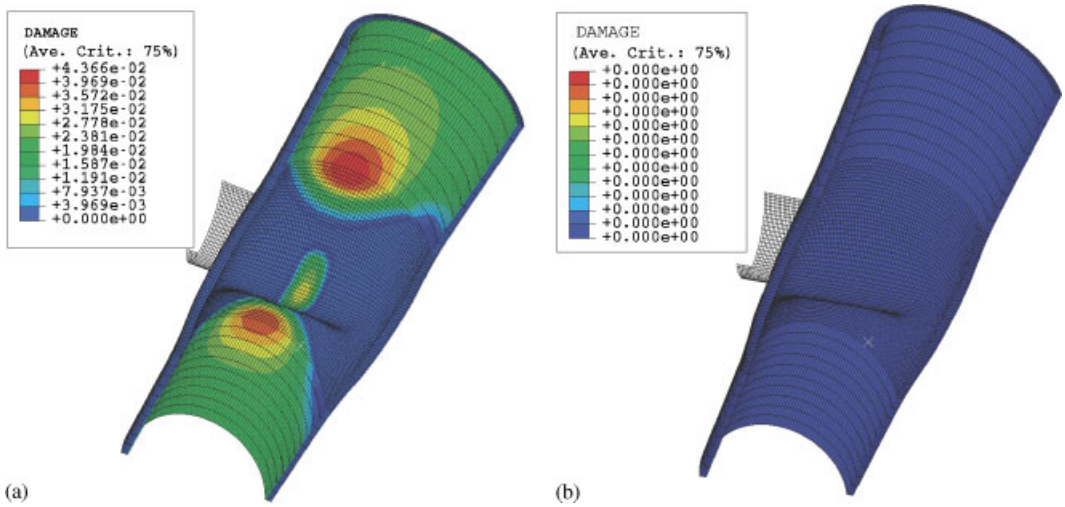

Figure 17. Damage distribution after clamping: (a) matrix damage; and (b) fibres damage.

of soft biological tissues. To simulate the damage properties of this kind of tissues, we consider different damage evolution for the matrix and the different families of fibres. Only the models proposed by Natali *et al*. [11] and Rodriguez *et al*. [15] consider uncoupled matrix and fibres damage for soft biological tissues.

Emphasis has been placed on the numerical treatment of the proposed formulation in the context of the finite element method and particular attention has been focused on the derivation of the corresponding consistent tangent tensor, essential for the solution of the implicit finite element equations. Our model differs from those proposed by Natali *et al*. [11] in which damage was characterized in their paper by the maximum value previously attained by the stretch of the undamaged material. This results in a non-symmetric algorithmic tangent modulus with a high computational cost.

At the fibre level, our model differs from that proposed by Rodriguez *et al*. [15] in which they use the statistical distribution of the length of collagen fibres to define the damage model for the reinforcing material. However, that model requires to solve the integration of the probability density function, and to obtain the parameters of such statistical distribution which is very complex in general and needs structural information difficult to obtain.

Several numerical examples under finite strains have been presented in order to illustrate the good performance and the physical mechanisms inherent to the constitutive model presented herein. In particular, we analyse several 3D simulations of the behaviour of the MCL under non-physiological valgus moment and a simplified artery during balloon angioplasty and clamping. Good qualitative agreement was found between the numerical and experimental results for the MCL and for the arterial examples, indicating that the constitutive damage model can capture the typical stress–strain behaviour observed in fibrous soft tissues.

REFERENCES

1. Fung YC. *Biomechanics. Mechanical Properties of Living Tissues*. Springer: Berlin, 1993.

DOI: 10.1002/nme

2. Holzapfel GA, Weizscker HW. Biomechanical behavior of the arterial wall and its numerical characterization. *Computers in Biology and Medicine* 1998; **28**:377–392.
3. Peña E, Martinez MA, Calvo B, Doblaré M. On the numerical treatment of initial strains in soft biological tissues. *International Journal for Numerical Methods in Engineering* 2006, in press, doi: 10.1002/nme.1726.
4. Weiss JA, Maker BN, Govindjee S. Finite element implementation of incompressible, transversely isotropic hyperelasticity. *Computer Methods in Applied Mechanics and Engineering* 1996; **135**:107–128.
5. Pioletti DP, Rakotomanana L. Finite element model of the anterior cruciate ligament. *European Journal of Mechanics – A/Solids* 2000; **19**:749–759.
6. Peña E, Calvo B, Martinez MA, Doblaré M. A three-dimensional finite element analysis of the combined behavior of ligaments and menisci in the healthy human knee joint. *Journal of Biomechanics* 2006; **39**:1686–1701.
7. Holzapfel GA, Gasser TC, Ogden RW. A new constitutive framework for arterial wall mechanics and a comparative study of material models. *Journal of Elasticity* 2000; **61**:1–48.
8. Alastrue V, Calvo B, Peña E, Doblare M. Biomechanical modelling of refractive corneal surgery. *Journal of Biomechanical Engineering* (ASME) 2006; **128**.
9. Hurschler C, Loitz-Ramage B, Vanderby R. A structurally based stress-strech relationship for tendon and ligament. *Journal of Biomechanical Engineering* 1997; **119**:392–399.
10. Liao H, Belkoff SM. A failure model for ligaments. *Journal of Biomechanics* 1999; **38**:183–188.
11. Natali AN, Pavan PG, Carniel EL, Luisiano ME, Taglialavoro G. Anisotropic elasto-damage constitutive model for the biomechanical analysis of tendons. *Medical Engineering and Physics* 2005; **27**:209–214.
12. Hokanson J, Yazdami S. A constitutive model of the artery with damage. *Mechanics Research Communications* 1997; **24**:151–159.
13. Arnoux PJ, Chabrand P, Jean M, Bonnoit J. A visco-hyperelastic with damage for the knee ligaments under dynamic constraints. *Computer Methods in Biomechanics and Biomedical Engineering* 2002; **5**:167–174.
14. Schechtman H, Bader DL. Fatigue damage of human tendons. *Journal of Biomechanics* 2002; **35**:347–353.
15. Rodríguez J-F, Cacho F, Bea JA, Doblaré M. A stochastic-structurally based three dimensional finite-strain damage model for fibrous soft tissue. *Journal of the Mechanics and Physics of Solids* 2006; **54**:564–886.
16. Provenzano PP, Heisey D, Hayashi K, Lakes R, Vanderby Jr R. Subfailure damage in ligament: a structural and cellular evaluation. *Journal of Applied Physiology* 2002; **92**:362–371.
17. Lemaitre J. A continuous damage mechanics model for ductile fracture. *Journal of Biomechanical Engineering* (ASME) 1985; **107**:83–89.
18. Simo JC, Ju JW. Strain- and stress-based continuum damage models. I. Formulation. *International Journal of Solids and Structures* 1987; **23**:821–840.
19. Simo JC, Ju JW. Strain- and stress-based continuum damage models. II. Computational aspects. *International Journal of Solids and Structures* 1987; **23**:841–870.
20. Simo JC. On a fully three-dimensional finite-strain viscoelastic damage model: formulation and computational aspects. *Computer Methods in Applied Mechanics and Engineering* 1987; **60**:153–173.
21. Govindjee S, Simo JC. Mullins' effect and the strain amplitude dependence of the storage modulus. *International Journal of Solids and Structures* 1992; **29**:1737–1751.
22. Souza Neto EA, Peric D, Owen DRJ. Continuum modelling and numerical simulation of material damage at finite strains. *Arch Comput Method Eng* 1998; **5**:311–384.
23. Spencer AJM. Theory of invarinats. *Continuum Physics*. Academic Press: New York, 1954; 239–253.
24. Humphrey JD. Continuum biomechanics of soft biological tissues. *Proceedings of the Royal Society of London, Series A* 2002; **175**:1–44.
25. Simo JC, Taylor RL. Quasi-incompressible finite elasticity in principal stretches. Continuum basis and numerical algorithms. *Computer Methods in Applied Mechanics and Engineering* 1991; **85**:273–310.
26. Holzapfel GA. *Nonlinear Solid Mechanics*. Wiley: New York, 2000.
27. Flory PJ. Thermodynamic relations for high elastic materials. *Transaction of the Faraday Society* 1961; **57**: 829–838.
28. Simo JC, Taylor RL. Consistent tangent operators for rate-independent elastoplasticity. *Computer Methods in Applied Mechanics and Engineering* 1985; **48**:101–118.
29. Marsden JE, Hughes TJR. *Mathematical Foundations of Elasticity*. Dover: New York, 1994.
30. Simo JC, Hughes TJR. *Computational Inelasticity*. Springer: New York, 1998.
31. Naghdi PM, Trapp JA. The significance of formulating plasticity theory with reference to loading surfaces in strain space. *Italian Journal of Engineering Science* 1975; **13**:785–797.
32. Gardiner JC. Computational modeling of ligament mechanics. *Ph.D. Thesis*, The University of Utah, 2002.

DOI: 10.1002/nme

33. Hull ML, Berns GS, Varma H, Patterson A. Strain in the medial collateral ligament of the human knee under single and combined loads. *Journal of Biomechanics* 1995; **29**:199–206.
34. Provenzano PP, Hayashi K, Kunz DN, Markel MD, Vanderby R. Healing of subfailure ligament injury: comparison between immature and mature ligaments in a rat model. *Journal of Orthopaedic Research* 2002; **20**:975–983.
35. Weiss JA. A constitutive model and finite element representation for transversely isotropic soft tissues. *Ph.D. Thesis*, The University of Utah, 1994.
36. Limbert G, Middleton J. A transversely isotropic viscohyperelastic material. Application to the modeling of biological soft connective tissues. *International Journal of Solids and Structures* 2004; **41**:4237–4260.
37. Fu FH, Harner C, Vince KG. In *Knee Surgery*. Willians & Wilkins: Baltimore, MD, 1994.
38. Daniels DM. *Knee Ligaments*: *Structure*, *Function*, *Injury and Repair*. Raven Press: New York, 1990.
39. Humphrey JD. Mechanics of the arterial wall: review and directions. *Critical Reviews in Biomedical Engineering* 1995; **23**:1–162.
40. Gasser TC, Holzapfel GA. A rate-independent elastoplastic constitutive model for (biological) fiber-reinforced composites at finite strains: continuum basis, algorithmic and finite element implementation. *Computational Mechanics* 2002; **29**:340–360.
41. Holzapfel GA, Stadler M, Schulze-Bauer CAJ. A layer specific three-dimensional model for the simulation of balloon angioplasty using magnetic resonance imaging and mechanical testing. *Annals of Biomedical Engineering* 2002; **30**:753–767.
42. Oktay HS. Continuum damage mechanics of ballon angioplasty. *Internal Report*, *U.M.I.*, 1993.
43. Ogden RW, Roxburgh DG. A pseudo-elastic model for the Mullins' effect in filled rubber. *Proceedings of the Royal Society of London*, *Series A* 1999; **455**:2861–2877.
44. Gasser TC, Schulze-Bauer CAJ, Holzapfel GA. A three-dimensional finite element model for arterial clamping. *Journal of Biomechanical Engineering* (ASME) 2002; **124**:355–363.
45. Chu B, Blatz P. Cumulative microdamage model to describe the hysteresis of living tissue. *Annals of Biomedical Engineering* 1972; **1**:204–211.
46. Margovsky AI, Chambers AJ, Lord RS. The effect of increasing clamping forces on endothelial and arterial wall damage: an experimental study in the sheep. *Cardiovascular Surgery* 1999; **7**:457–463.

DOI: 10.1002/nme